Shoulder Biomechanics of Pushrim Impact during Wheelchair Propulsion in Tetraplegia: A Case Report

SA Sisto[1,2], M Yarossi[1], G Forrest[1,2], AM Kwarciak[1], J Cole[2,3], T Dyson-Hudson[1,2], ML Boninger[3], S Kirshblum[1,2,4]
[1]Kessler Medical Rehabilitation Research and Education Corporation, 1199 Pleasant Valley Way, West Orange, NJ 07052
[2]University of Medicine and Dentistry/New Jersey Medical School, Department of Physical Medicine &Rehabilitation
[3]Human Engineering Research Laboratories, University of Pittsburgh, Pittsburgh, PA 15206
[4]Kessler Institute for Rehabilitation, 1199 Pleasant Valley Way, West Orange, NJ 07052

Introduction

Prolonged manual wheelchair use has been thought to cause repetitive strain injuries that produce a nearly 31-73% prevalence of upper limb pain.[1] Some researchers have suggested that damage to the upper limb may be functionally and economically equivalent to a spinal cord injury (SCI) of higher neurological level.[2] While an increasing number of studies have evaluated individuals with paraplegia, few have evaluated individuals with tetraplegia (IWT), who have a high prevalence of shoulder pain.[2] Due to impaired hand function, IWT often use a striking motion to propel the wheelchair. Robertson et al.[5] hypothesized that pushrim impact could cause rapid loading of the joint structures possibly producing joint trauma. The aim of this study was to compare pushrim kinetics to the forces, moments and EMG of the shoulder, during initial pushrim contact for 2 IWT. This information may help identify the biomechanical factors related to shoulder pain and pathology, as well as aid in the setup of manual wheelchairs.

Methods

Participants included two males, ages 46 and 41, with a C6 motor complete injury. Both participants described their shoulder pain as minimal or non-existent and had no known shoulder pathology. Each participant was asked to propel his wheelchair on a custom-built roller system at a comfortable self-selected speed for 20 seconds. Data collection began when the participant verbalized he had reached a steady speed. Anthropomorphic measures were taken of each segment.

Three-dimensional (3D) kinematic data were collected at 120 Hz using a passive marker motion capture system (Vicon Motion Systems, Oxford). Reflective markers were placed on each wheel and on bony landmarks on the upper limbs and trunk in accordance to the ISB recommendations.[3]

Stainless steel nickel alloy insulated fine wire electrodes were inserted into 13 muscles of the right upper arm and scapula and each was attached to one pole of a pre-amplified electrode. The second pole was attached to an Ag/AgCl surface electrode placed on the skin over the muscle (except the subscapularis, for which a second intramuscular electrode was inserted). All signals were amplified and low-pass filtered at 1250 Hz by the EMG collection unit (Motion Lab Systems, Baton Rouge, LA) and passed to the Vicon Workstation as an analog input. EMG data were recorded at 2520 Hz.

Kinetic data were collected at 240 Hz from two SmartWheels (Three Rivers Holdings, LLC, Mesa, AZ), which replaced the rear wheels of the wheelchair during testing. The SmartWheel has an instrumented pushrim that measures 3D forces and moments along and about the anterior-posterior, vertical, and medial-lateral directions.

Data Reduction and Analysis

Data from 10 consecutive right-sided push strokes were selected for analysis. The push cycle was defined as the start of one push phase (when the moment about the axle exceeded two standard deviations above the resting amplitude) to the start of the next. Five specific events in the push cycle were identified for further analysis based upon the shoulder flexion/extension moment (Figure 1). The initial event, P1, represents the point at which maximum shoulder extension moment occurs. Events P2-P5 were defined as the 'impact phase' of the push cycle. All signals were

06-3054

analyzed using custom routines written in Matlab (MathWorks, Natick, MA).

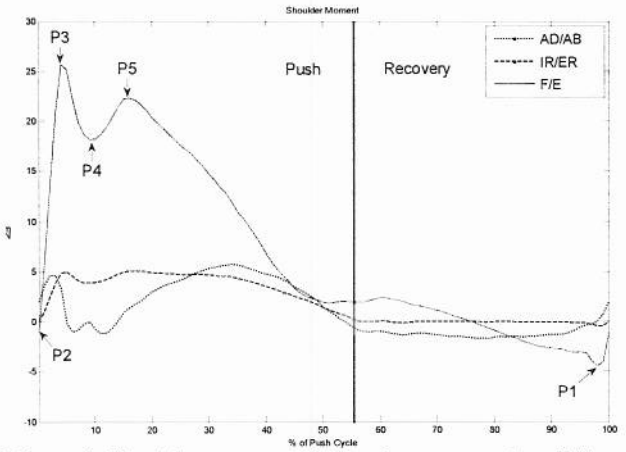

Figure 1. Shoulder moments during the mean stroke of N1. Labeled events:
P1: Maximum shoulder extension moment.
P2: 1ms after contact with the pushrim.
P3: The first peak after contact (impact spike).
P4: Valley after impact caused by rebound off the rim.
P5: First peak after rebound (push peak).

EMG analysis

Visual inspection of quiet EMG activity was used to establish baseline signal amplitude. Data were full wave rectified; and three standard deviations above the baseline for a period of 50 ms was defined as active EMG.[4] A root mean square average was applied to create a linear envelope of the signal. The linear envelope was normalized to the mean amplitude of the greatest one-second of muscle activity during a maximum voluntary contraction.

Kinematic Analysis

Kinematic data were filtered using a 4th order low pass Butterworth filter with a 7 Hz cutoff frequency. The upper limb was modeled as three connected rigid body segments to represent the hand, forearm, and upper arm. Each segment was described using the ISB recommended local coordinate system and Euler ('zxy' order) angle-defined segment orientations. The distal segment was rotated to the proximal segment (humerus to the trunk) to represent the anatomical angles for the shoulder, elbow, and wrist. All joint angles were equal to zero at neutral seated position (arms at the sides with the forearm at 90 degrees to the humerus, palms facing medially, and fingers pointing forward).

Anthropomorphic model

The forearm and upper arm were modeled as truncated circular cones and the hand was modeled as a semi-ellipsoid. Mass, center of mass, and moment of inertia were determined using the body segment parameter equations.[6]

Kinetic Analysis

3D forces obtained from the SmartWheel were projected onto the hand. The point of force application was defined as halfway between the wrist center and the hand center of mass, placing it at the base of the palm. This point was consistent with visual observations of pushrim contact. Inverse dynamic equations[7] were used to find forces and moments at the shoulder. At the pushrim, Cartesian force components were converted into tangential, radial, and axial forces, as well as summed to find the resultant force.

Results

Stroke Style

Participant 1 (N1) used a pumping style[8] push stroke, while participant 2 (N2) used a double-looping over propulsion stroke pattern (Figure 2).

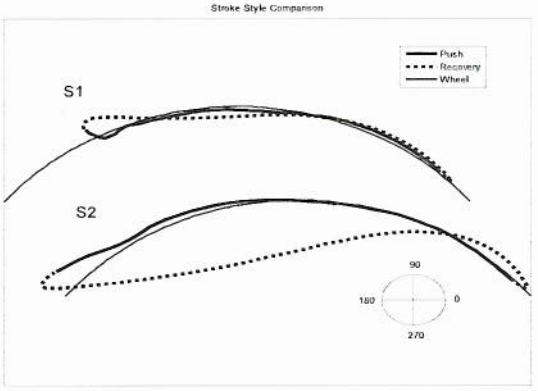

Figure 2. Mean stroke trajectory for each participant.

N1 contacted the rim at 118.3° and had an average push angle of 67° (covering 15.9° from P2 to P5). N2 contacted the pushrim at 130° and had an average push angle of 76° (covering 24° from P2 to P5). Mean self-selected speeds for N1 and N2 were 0.71 m/s and 1.2 m/s respectively.

Table 1: Key variables at each impact phase event

	P2 Initial Contact	P3 Impact Spike	P4 Rebound	P5 Push Peak
Participant 1				
Pushrim				
Hand angle (°)	119.4	117.4	112.0	103.5
F_{total} (N)	19.6	105.7	87.3	112.6
F_{tan} (N)	0.2	22.7	20.3	35.0
F_{rad} (N)	14.7	77.8	61.0	72.1
F_{ax} (N)	-4.8	1.4	5.9	5.5
Eff (F_{tan}/F_{total})*	0.9	21.5	23.3	31.1
Shoulder				
F_x (N) ant/post	-2.8	-53.2	-41.1	-53.2
F_y (N) sup/inf	-22.9	23.7	12.2	22.7
F_z (N) med/lat	4.8	-1.4	-5.9	-5.5
M_x (Nm) flex/ext	-1.1	25.6	18.2	22.3
M_y (Nm) IR/ER	0.0	4.9	3.8	5.0
M_z (Nm) add/abd	2.0	3.3	0.0	1.4
Participant 2				
Pushrim				
Hand angle (°)	128.9	119.0	114.4	104.7
F_{total} (N)	25.9	110.9	108.7	147.3
F_{tan} (N)	0.3	31.8	34.1	50.3
F_{rad} (N)	19.1	70.6	70.5	79.8
F_{ax} (N)	-6.5	-8.5	-4.0	-17.1
Eff (F_{tan}/F_{total})*	1.1	28.7	31.4	34.2
Shoulder				
F_x (N) ant/post	-11.2	-63.4	-62.4	-75.2
F_y (N) sup/inf	-23.7	5.3	8.3	17.9
F_z (N) med/lat	6.5	8.5	4.0	17.1
M_x (Nm) flex/ext	2.2	27.7	26.2	29.0
M_y (Nm) IR/ER	0.2	5.6	6.0	7.4
M_z (Nm) add/abd	3.1	6.8	4.9	11.0

*Eff = efficiency; negative numbers correspond to the latter direction (e.g. posterior, lateral, extension, etc.).

Figure 3 shows the mean angles and kinetics during pushrim impact. N2 contacted the pushrim in more shoulder hyperextension (41.4°) then N1 (24.3°). During the impact phase both N1 and N2 had lower tangential pushrim forces compared to radial forces, which are directed towards the hub. Between P2 and P3, N1 tangential force decreased from 22.7 N to 20.3 N while N2 tangential force increased from 31.8 N to 34.1 N. The total force on the wheel from P3 to P4 dropped much less for N2 (~111 to109 N) than for N1 (~106 to 87 N). From P3 to P5 radial force represented a larger percentage of the total force on the pushrim for N1. N2 axial force was of greater magnitude than N1 and directed towards the body. N1 applied an axial force away the body from P3 to P5. In terms of efficiency (F_{tan}/F_{total}), N2 maintained a higher ratio (.29-.34) than N1 (.22-31) from P3-P5.

Regarding shoulder forces and moments, N1 had a greater superior directed force (23.7 N) at peak impact (P3) compared to N1 (5.3 N). F_z was directed medially for N1 and laterally for N2. N1 contacted the pushrim with an extension moment (-1.1 Nm), whereas N2 has already developed a flexion moment (2.2 Nm). N2 also had a larger adduction moment from P2-P5 than N1.

N1 EMG data showed the anterior deltoid muscle firing at a higher percentage of the MVC than the pectoralis muscle during the impact phase while the converse was true for N2. Both participants had maximal firing of the sub-scapularis throughout impact phase (Figure 4).

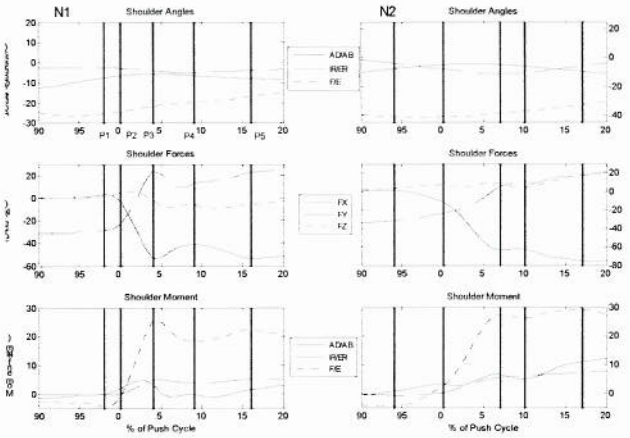

Figure 3. Mean shoulder angles, forces and moments (bottom) during pushrim impact; where flexion, adduction, and internal rotation are all positive.

Discussion

Unable to grab the pushrim to pull with the biceps and lacking the triceps innervations to push by extending the elbow, individuals with hand impairments must produce a radial and axial force of greater magnitude than the tangential force to maintain adequate contact between the hand and the pushrim throughout propulsion.

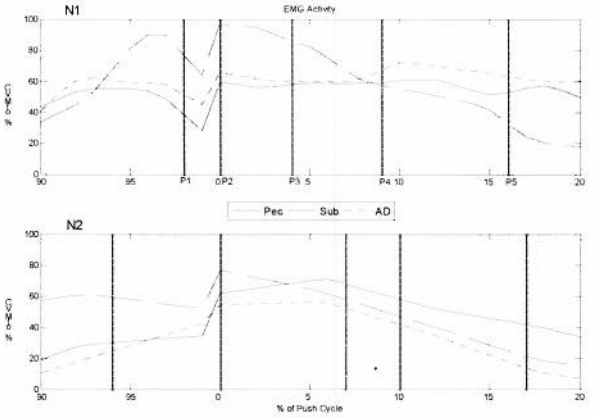

Figure 4. EMG activity of the pectoralis, anterior deltoid, and subscapularis muscles during pushrim impact. MVC of the subscaplualris exceeded 100% and was scaled down by a factor of 1.7 for convenient plotting.

At P2, N1 dropped the hands down to the pushrim with a shoulder extension moment, while N2 contacted the pushrim from behind, with a shoulder flexion moment. For N1, this lead to slower speed, lower efficiency, and a higher stroke frequency.

Specifically at P2, but throughout the entire impact phase, the compressive forces of the shoulder of N1 were greater than those of N2. Compressive forces in the shoulder, which are thought to have the greatest correlation to subacromial impingement,[9] are those directed superiorly and medially, forcing the head of the humerus into the joint. It is suspected that N2 had lower compressive forces due to an initially smaller radial force on the pushrim, a larger axial force, and more extension of the shoulder. N2 was able to supplement the radial force needed to maintain contact with the pushrim by pushing with a larger, medially-directed axial force. This force, which correlated with an increased shoulder adduction moment, resulted in non-compressive lateral force at the shoulder. The increased shoulder adduction moment was achieved by using the pectoralis (adductor and flexor) at a more maximal level than the anterior deltoid (flexor). Finally, although radial forces for N2 were greater than or equal to those for N1, the smaller superior forces on the shoulder may be due to differences in limb position resulting from greater shoulder hyperextension.

Limitations

The use of the acromion to represent the gleno-humeral joint center may have introduced error into calculations. Also, the use of a 'zxy' rotation to calculate shoulder flexion/extension differs from ISB standards. Finally, shoulder motion was determined without consideration of the scapula.

Conclusions

Though they possess similar levels of motor function, N1 and N2 demonstrated two different wheelchair propulsion techniques of IWT. It appeared that contacting the pushrim from behind and using shoulder adduction to gain the necessary frictional force for propulsion reduced the amount of compressive force (F_y) on the glenohumeral joint. It also allowed for a more efficient push stroke by minimizing the loss in tangential force on the pushrim during rebound (P4). In order to obtain the necessary adduction moment, the pectoralis should be strengthened and wheelchair setup optimized to favor the use of the pectoralis over the anterior deltoids. Further research will evaluate distal segments and the relationship of all variables to scapular EMG, radiological and physical examination for pathology of the shoulder, and wheelchair fit.

REFERENCES

1. Curtis KA, Drysdale GA, Lanza RD, et al. Shoulder pain in wheelchair users with tetraplegia
2. Sie I, Waters R, Adkins R, et al. Upper extremity pain in the post-rehabilitation spinal cord injured patient. *Archives of Physical Medicine & Rehabilitation*, 1992;44-8.
3. Wu, G, van der Helm, FCT, Veeger, DJ, et al. ISB recommendations on definitions of joint coordinate systems of various joints for the reporting of human joint motion—Part II: shoulder, elbow, wrist and hand. *Journal of Biomechanics*, 2005, 38:981-92.
4. Konrad, P. The ABC of EMG: A practical Introduction to Kinesiological Electromyogrphy, Version 1.0, Apr, 2005, Noraxon
5. Robertson, RN, Boninger, ML, Cooper RA, et al. Pushrim forces and joint kinetics during wheelchair propulsion. *Archives of Physical Medicine and Rehabilitation*, 1996,77:856-64.
6. Yeadon, MR The simulation of aerial movement-II. A mathematical inertia model of the human body. *Journal of Biomechanics*, 1990, 23,:67-74.
7. Requejo, PS, Wahl, DP, Bontrager, EL, et al. Upper extremity kinetics during lofstrand crutch-assisted gait. *Medical Engineering & Physics*, 2005,27:19-29.
8. Shimada, SD, Robertson, RN, Boninger, ML, et al. Kinematic characterization of wheelchair propulsion. *Journal of Rehabilitation Research and Development*, 1998, 35(2):210-18.
9. Kulig, K, Newsam, CJ, Mulroy, SJ, et al. The effect of level of spinal cord on shoulder joint kinetics during manual wheelchair propulsion. Clinical Biomechanics, 2001, 16:744-751.